AIP Advances

Violet-blue photoluminescence from Si nanoparticles with zinc-blende structure synthesized by laser ablation in liquids

P. Liu, Y. Liang, H. B. Li, J. Xiao, T. He, and G. W. Yang

Citation: AIP Advances **3**, 022127 (2013); doi: 10.1063/1.4794203
View online: http://dx.doi.org/10.1063/1.4794203
View Table of Contents: http://scitation.aip.org/content/aip/journal/adva/3/2?ver=pdfcov
Published by the AIP Publishing

AIP ADVANCES **3**, 022127 (2013)

Violet-blue photoluminescence from Si nanoparticles with zinc-blende structure synthesized by laser ablation in liquids

P. Liu,[a] Y. Liang, H. B. Li, J. Xiao, T. He, and G. W. Yang[b]
State Key Laboratory of Optoelectronic Materials and Technologies, Institute of Optoelectronic and Functional Composite Materials, Nanotechnology Research Center, School of Physics & Engineering, Sun Yat-sen University, Guangzhou 510275, Guangdong, P. R. China

(Received 25 October 2012; accepted 14 February 2013; published online 28 February 2013)

Violet-blue luminescence from Si nanostructures has been widely investigated, because of its potential use in optoelectronic and bioimaging devices. However, the emission mechanism in multiform Si nanomaterials remains unclear. In this contribution, Si nanocrystals (NCs) with zincblende structure and visible violet-blue emission are prepared by electric field assisted laser ablation in liquids. While subsequent annealing of the Si NCs weakens their blue emission dramatically. We investigate the origin of the violet-blue emission by monitoring crystal structure transitions and photoluminescence during different treatments of the Si NCs. The results indicate that the violet-blue emission cannot simply be ascribed to quantum confinement effects or the presence of general surface states on the Si NCs. Instead, we propose that excitons are formed within the Si NCs by direct transitions at Γ or X points, which can be induced during the formation of the zincblende structure, and are a most possible origin of the violet-blue luminescence. Furthermore, defects in the metastable Si NCs are also expected to play an important role in violet-blue emission. This study not only gives clear and general insight into the physical origins of violet-blue emission from Si NCs, it also provides useful information for designing optoelectronic devices based on Si NCs. [http://dx.doi.org/10.1063/1.4794203]

I. INTRODUCTION

Silicon (Si) products have been extensively investigated during the last 50 years and are currently the dominant semiconductor used in microelectronics and solar cells. With the development of nanotechnology, numerous low-dimensional Si nanomaterials have been synthesized in the last 20 years.[1–4] Si nanomaterials possess unique physical and chemical properties, such as size confinement and high surface area, and are of growing interest to researchers. Si nanomaterials may be applied in field-emission devices, biomedical imaging, biosensors, and energy storage.[5–7] Understanding the luminescent properties of Si nanomaterials and their underlying mechanisms are both major challenges that are currently being investigated because of their potential use in fundamental physics and optoelectronics applications.[8–10] Many researchers have focused their attention on the emission characteristics of various Si nanostructures,[4,8,11,12] and luminescent Si nanoparticles have received particular interest.[13–15] Research of Si nanoparticles exhibiting visible emission will greatly benefit silicon-based optoelectronics, full color displays, and biotechnology.[7,16–18] However, there have been few in-depth studies investigating the origin of luminescence from Si nanomaterials, and reports of violet-blue light emission from Si nanocrystals are scarce.[19,20]

[a]Electronic mail: liupu5@mail.sysu.edu.cn, Tel.: +86-20-8411-5943
[b]Author to whom correspondence should be addressed. Email: stsygw@mail.sysu.edu.cn, Tel. and Fax.: +86-20-8411-3692

The emission mechanism and detailed origin of the photoluminescence (PL) in Si nanoparticles are controversial, and at least four main pathways for emission have been proposed, including: (i) quantum size confinement effects,[21,22] (ii) direct band gap emission related to the ultrasmall size of Si,[23] (iii) oxide-related effects,[24,25] and (iv) surface state or stacking fault-induced emission effects.[26,27] Recently, Zeng *et al.*[20] proposed a mechanism where some excitons form and are trapped by nonradiative Pb centers within Si nanocrystals (NCs), and others recombine in the area between Si and the surrounding SiO_x, to explain the blue emission from their Si nanoparticles. Here, we question whether there are other mechanisms apart from those mentioned above that can explain the origin of violet-blue luminescence in Si nanomaterials.

In this contribution, we synthesize Si NCs with a zincblende structure that emits violet-blue light using electric field-assisted laser ablation in liquids (EFLAL). The Si NCs are characterized by scanning electron microscopy (SEM), X-ray diffraction (XRD), transmission electron microscopy (TEM), energy-dispersive X-ray spectroscopy (EDS), absorption spectroscopy, PL measurements and Raman spectroscopy. Annealing treatment studies are also performed to probe the relationship between structure and PL in these Si NCs.

II. EXPERIMENTAL

Techniques based on the interaction of a pulsed laser with materials in a liquid environment have attracted substantial interest in the past few years and have been applied in diverse fields from micromachining to NC synthesis.[28–40] More recently, there have been several experimental reports on using laser ablation in liquids (LAL) to trap metastable phases.[41–44] Based on this method, a facile technique called EFLAL has been developed, which enables controlled fabrication of micro- and nanostructures with metastable structures without using any catalyst or organic additives (*i.e.*, it is a 'green' synthesis method).[45] Herein, we provide details of an improved synthetic procedure based on EFLAL, which is depicted schematically in Fig. 1. A single-crystalline Si target with diamond-type structure and 99.999% purity was used as the starting material. The target was held in a polytetrafluoroethylene fitting and suspended at one end of a rectangular quartz chamber with dimensions of 10.0 × 4.0 × 3.0 cm. Two parallel square graphite electrodes separated by a distance of 3.3 cm were placed next to the target to provide a dc electric field of 120 V. The chamber was filled with ultra-pure water (resistance 18.2 MΩ) that was maintained at room temperature during the experiment. High power laser pulses from two harmonic Q-switched Nd:YAG lasers (wavelength 532 nm, pulse width 10 ns, power density 10^{11} W/cm^2, and repetition frequency 2.5 Hz) were finely focused on the target surface. A magnetic stirrer was used to disperse the fine particles generated during the process, and the whole chamber system was placed on an E-motion surface, which moved the Si target horizontally at slow speed during the laser ablation process. After the laser pulse was applied to the target for 120 min, the gray-white powder generated was collected from the chamber and dried at 50 °C in a vacuum oven. The drying process did not change the crystalline structure of the product.

The Si NCs synthesized by laser ablation were examined by SEM (JSM-6330F, 150 kV) and high-resolution transmission electron microscopy (HRTEM, JEM-2010F, 200 KV) on copper grids with carbon supports. Raman scattering measurements were carried out under 514.5 nm excitation from an Ar-ion laser line using a Renishaw inVia+Plus laser microRaman system (maximum laser power 20 mW, 500× objective). Si NCs were deposited on pure quartz substrates for XRD, Raman scattering, PL, and UV absorption measurements. All characterization measurements were obtained at room temperature in air.

III. RESULTS AND DISCUSSION

A. Morphology and structure characterization of Si NCs

Typical SEM images of the as-synthesized Si NCs are shown in Fig. 2. Most of the spherical micro- and nanoparticles are uniform in size and possess rough surfaces, with an average diameter of 40–60 nm (Fig. 2(b)). Interestingly, the high-magnification SEM image shown in the inset of

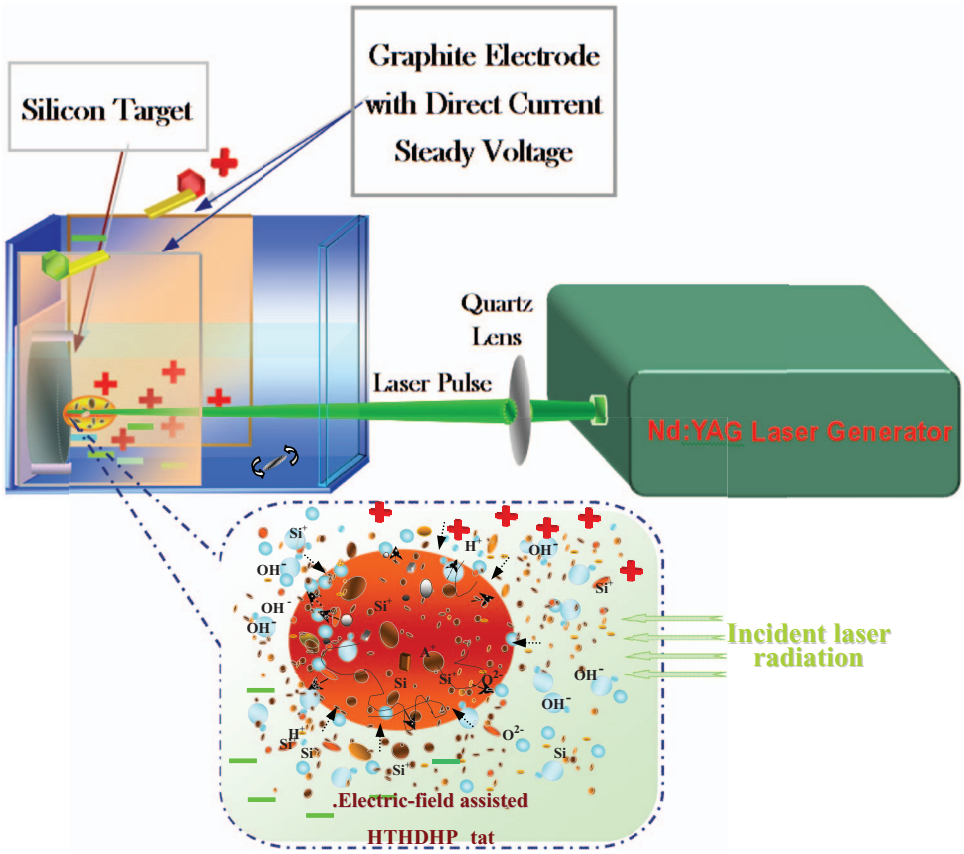

FIG. 1. Schematic illustration of electrical field assisted laser ablation in liquid (EFLAL) and its fabrication mechanism.

Fig. 2(a) reveals both micro- and nanosized crystals with an average diameter of 200 nm and rough surfaces. Fig. 2(c) shows the larger Si NCs consist of a main body in which many smaller NCs are embedded. A recent report indicated that the bimodal size distribution of nanoparticles formed by LAL is governed by a sudden rise in solution concentration caused by plasma erosion of the surface upon bubble collapse.[46] However, the rough, NC-embedded morphologies differ considerably to others published,[47–49] which implies that EFLAL produces NCs with unique morphologies. An XRD pattern and EDS analysis (Fig. 2(d) and its inset) of the NCs clearly show that the fabricated micro- and nanoparticles contain a crystalline phase of pure Si. The three XRD peaks located at 28.64 47.62 and 56.51° correspond to the (111), (220), and (311) crystalline planes of the zincblende structure of Si, respectively (JCPDS Card File No. 800018). A weak, broad band located at about 23° is attributed to the quartz substrate and the presence of a small amount of amorphous Si. Because there are no diffraction peaks consistent with oxide phases in the XRD pattern, and the small Cu and C signals in the EDS spectrum originate from the underlying copper grid, we conclude that the synthesized Si samples are crystalline and of high purity.

To determine the crystalline phase and structure of the Si NCs in detail, TEM and HRTEM images and corresponding selected area electron diffraction (SAED) patterns were obtained, as shown in Fig. 3(a)–3(d). Fig. 3(a) and 3(c) show that two different morphologies are present in the samples (*cf.* Fig. 2). The HRTEM image of a single nanoparticle in Fig. 3(a) shows a multitude of saturated, thin regions in the lattice planes (marked with white circles). This result not only clarifies the structure shown in Fig. 2(b), it also implies that there should be many stacking fault defects or asymmetrical lattice structures existing in the NC.[50,51] From the magnified HRTEM image (shown in the inset), the interplanar spacings are 0.309 and 0.189 nm, which correspond to the *d* values of the (111) and (220) crystallographic planes of the zincblende structure of Si, respectively. The corresponding SAED pattern (Fig. 3(b)) confirms the above result and also identifies some very

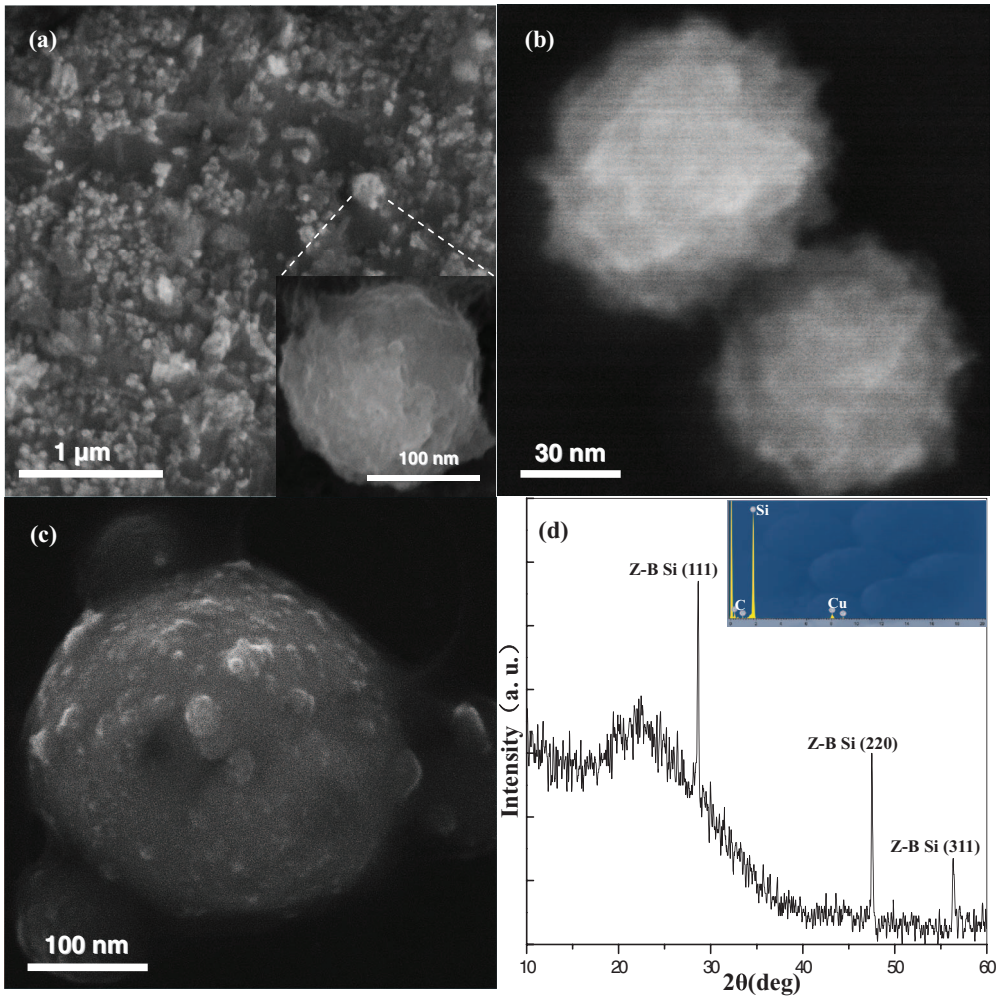

FIG. 2. (a) Low-magnification SEM image of the synthesized Si NCs. (b) High-magnification SEM image of two Si NCs. (c) High-magnification SEM image of Si NCs containing smaller embedded NCs. (d) XRD pattern of the synthesized Si NCs.

weak diffraction points (marked with white circles). We believe that these are caused by stacking fault defects or asymmetrical lattice structures in the NC. Fig. 3(c) shows a bright-field image of a large microcrystal, which has similar geometry to that of the particle in Fig. 2(c). An HRTEM image of the region indicated by a white rectangle in Fig. 2(c) reveals that the particle consists of several smaller NCs with a size of 7–14 nm. The interplanar spacings shown in Fig. 3(d) give *d* values of the lattice fringe of 0.265 and 0.310 nm. Note that the lattice spacing of 0.265 nm is the *d* value of the (200) crystallographic plane of the zincblende structure of Si, and cannot be seen in crystalline Si with a diamond-type structure. In the corresponding EDS (inset of Fig. 3(d)), the Si component was obtained with a measurement error of 2%, and the weak Cu and C peaks originate from the copper grid and amorphous carbon film support, respectively. Because almost no oxide layer is present on the Si samples (*cf*. HRTEM analysis above), the very weak O peak in the spectrum originates from the amorphous carbon film support. From the TEM images and XRD analysis, we conclude that the synthesized NCs consist of pure Si with a metastable zincblende structure.

B. Raman, PL measurements and UV absorption spectra

Raman spectra of the Si NCs were recorded under different laser power densities over a period of 10 s (Fig. 4). In the Raman spectrum obtained with a laser power density of 0.2 mW (Fig. 4(a)

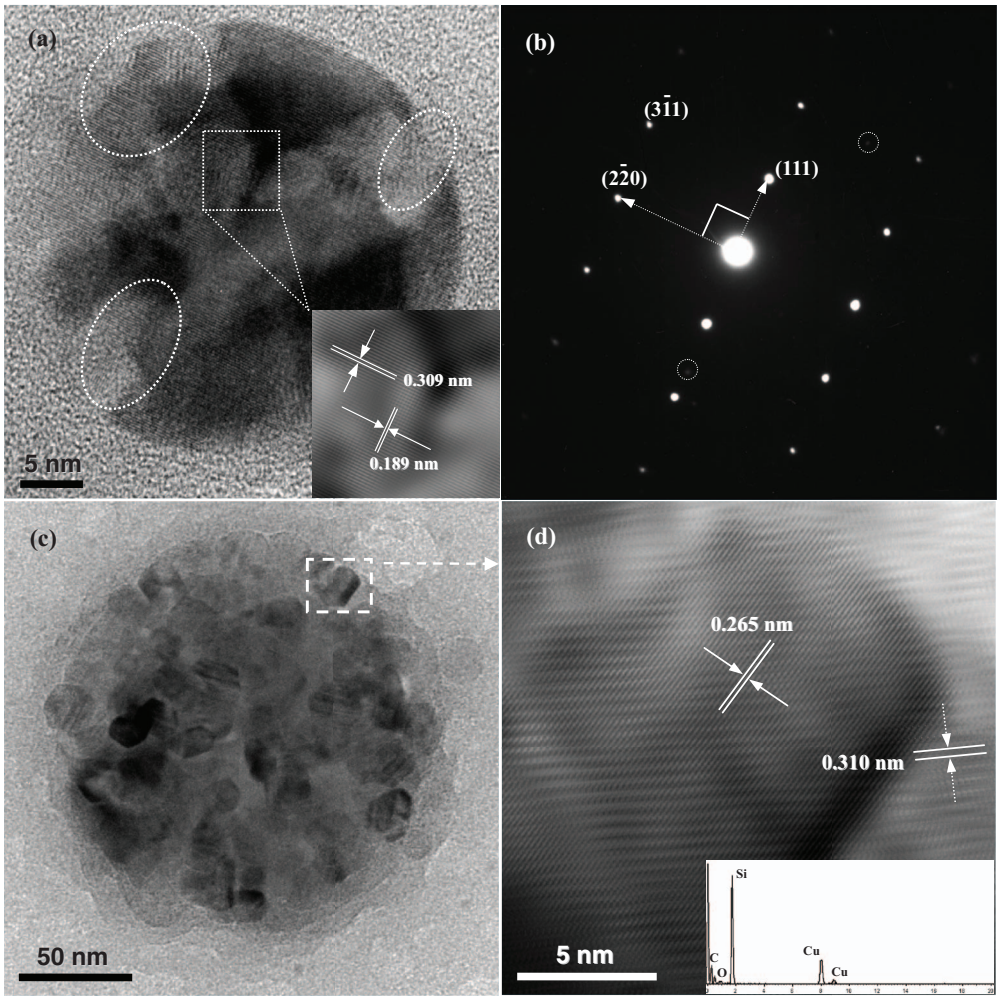

FIG. 3. (a) HRTEM image of Si NCs with stacking fault defects. (b) SAED pattern of Si NCs. (c) TEM and (d) HRTEM images of an Si NC.

pattern (i)), the strong peak at 520.17 cm^{-1} is consistent with the first-order Raman scattering band of crystalline Si, while the weak peak at 298.86 cm^{-1} is attributed to the 2TA(X) mode.[52] To the best of our knowledge, the Raman peak located at 298.86 cm^{-1} is very weak and hard to detect compared with the signal at 520.17 cm^{-1}. Therefore, it is difficult to simultaneously observe both the peaks at 520.17 and 298.86 cm^{-1} in the same spectrum.[52–54] The Raman spectrum recorded at high laser power density (1 mW, Fig. 4(a) pattern (ii)) exhibits peaks at 510.5 and 294.34 cm^{-1}. These peaks are both shifted to higher energy compared with those observed at low laser power density (Fig. 4(a) pattern (i)), and the peak at 294.34 cm^{-1} became very weak. Based on some previous reports,[51–55] we interpret the Raman spectra as follows: Si NCs normally exhibit a Raman shift because of the quantum size effect or heating effects from the detecting laser. In our case, however, most of the Si NCs are far too large to exhibit a quantum size effect, which is usually observed for nanoparticles of ~8 nm or smaller (*cf.* SEM and TEM analysis, and no obvious band broadening is found in the Raman scattering bands).[52,55] In addition, the laser power density used in Fig. 4(a) pattern (i) was very low (0.2 mW) and for a short period (10 s), so heating effects should be negligible. No Raman shift of the first-order Raman scattering band at 520.17 cm^{-1} can be seen in pattern (i), so the band at 298.86 cm^{-1} is assigned to the zincblende structure of the Si NCs. The NCs contain lattice mismatches or distortions, and the zincblende structure of Si is metastable, so it is reasonable to expect that the crystalline structure is sensitive to laser heating at high power densities

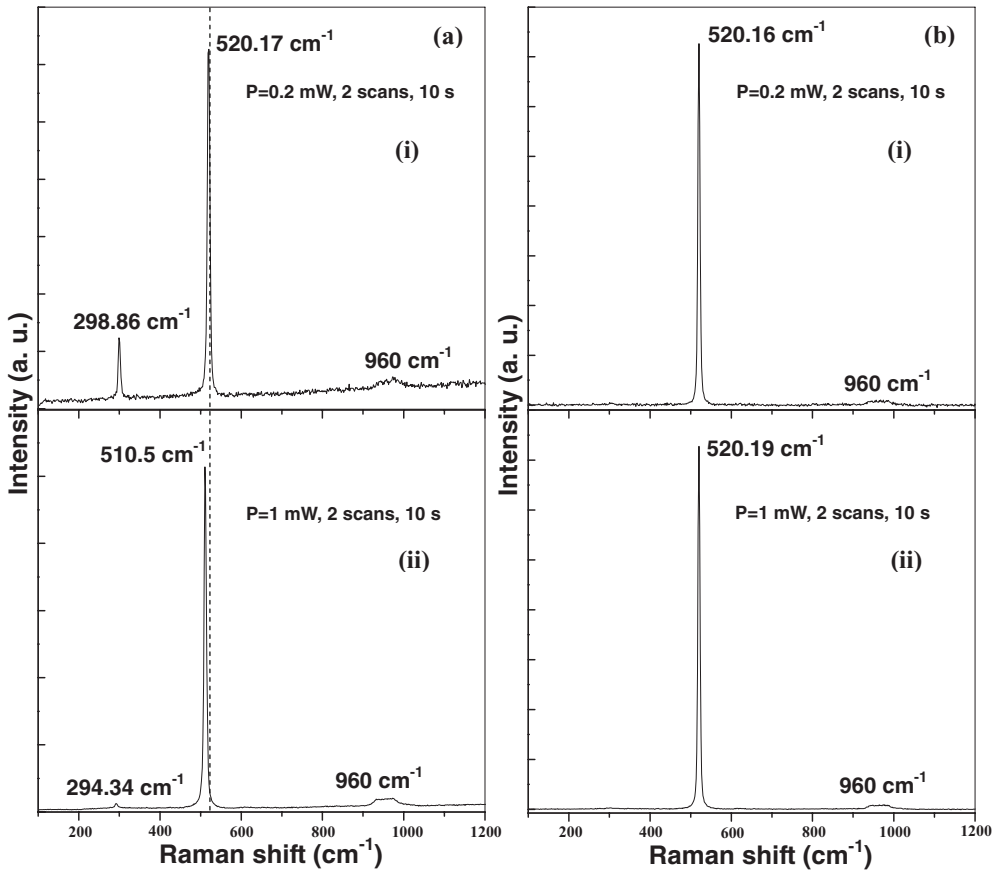

FIG. 4. Raman spectrum of (a) Si NCs and (b) single-crystalline Si target with diamond structure using laser power densities of (i) 0.2 mW, and (ii) 1 mW.

(1 mW, Fig. 4(a) pattern (ii)). That is, the crystalline defects observed in HRTEM analysis should contribute to the appearance and small shift of the Raman peak from 298.86 to 294.34 cm^{-1}.[51,52] Moreover, in our previous work,[51] the Raman spectra also showed very similar behavior to that in the Fig. 4(a) pattern (ii) in this work. Therefore, we believe that the Raman peak shifts to 510.5 cm^{-1} because of laser heating and scattering effects from the Si zincblende crystalline NCs containing defects.[52] Our analysis of the two Raman spectra in Fig. 4(a) is also consistent with XRD and TEM results. For comparison, Raman spectra of the original single-crystalline Si target with a diamond-type structure were recorded under the same conditions as that in Fig. 4(a), and are shown in Fig. 4(b). These spectra are identical and the peaks are consistent with single-crystalline Si, indicating that the typical diamond-type crystal structure of Si does not show obvious heating effects. These results further confirm that the Raman spectra in Fig. 4(a) originate from the metastable zincblende crystalline structure of Si.

The PL spectra of three typical Si NC samples are shown in Fig. 5(a). A dominant broad peak at 366 nm is observed in all spectra, along with a broad shoulder at 395 nm. In addition, a peak is observed at 324 nm in spectrum (ii) and a broad shoulder appears at 326 nm in spectrum (iii). No similar peak is observed in spectrum (i). Therefore, the emission peaks at about 324 and 395 nm are probably both caused by stacking fault defects or asymmetrical lattice structures present in the samples, because of their weak, variable emission behavior. Therefore, the Si NCs with a zincblende structure exhibit violet-blue emission at 366 nm, which has not been reported previously for Si NCs.[15,16,19,24,47,56–59] Although each PL spectrum exhibits a dominant peak at about 366 nm, the variable presence of minor peaks implies that there is possibly more than one origin of violet-blue emission in these Si NCs.

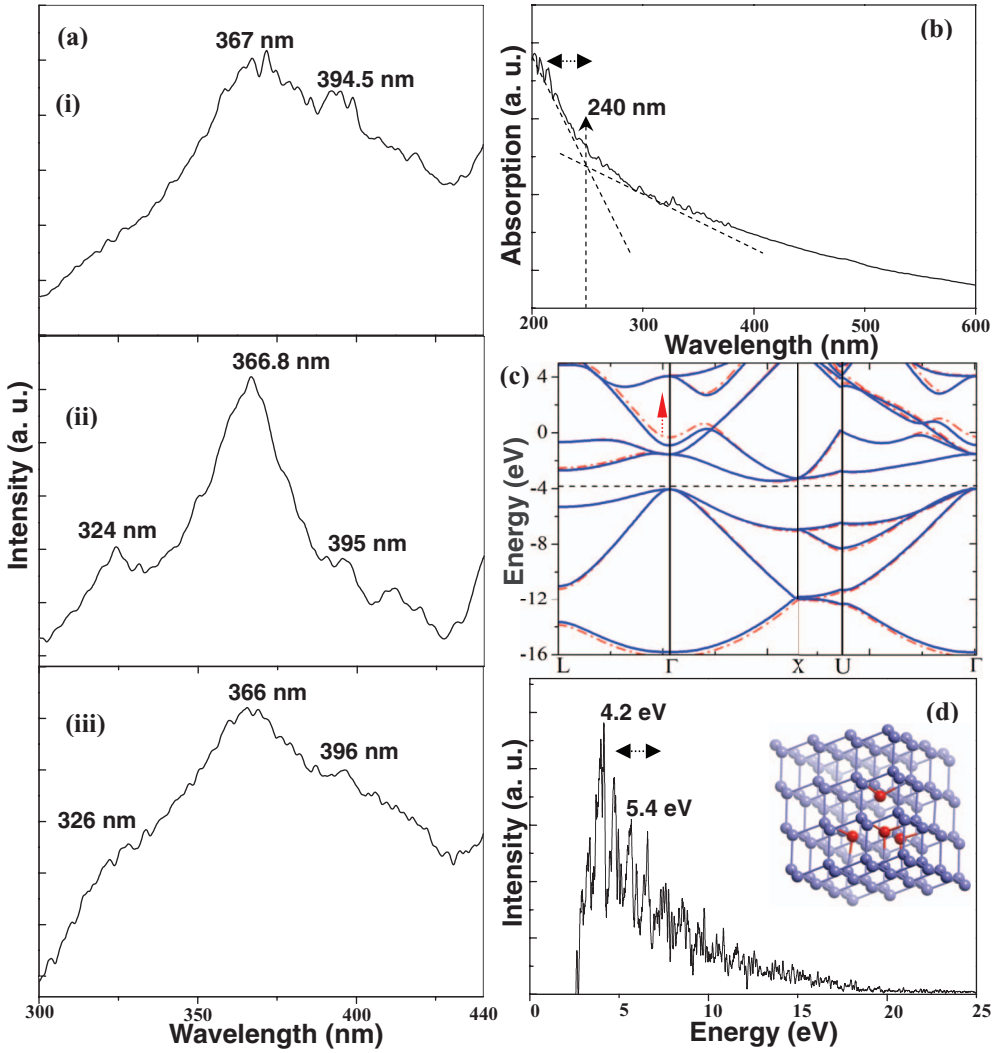

FIG. 5. (a) PL spectra of Si NCs produced by EFLAL (i–iii), and (b) UV absorption spectrum of the synthesized Si NCs. The calculated energy band structure of the Si NCs with a zincblende structure is shown in (c), and the corresponding absorption coefficient is calculated in (d).

A UV absorption spectrum of the synthesized Si NCs is shown in Fig. 5(b), and does not contain any obvious absorption peak. However, analysis of the UV curve revealed a weak absorption band that can be assigned from the intersection of two tangent line equations fitted to the data gained in the UV absorption spectrum. The intersection of the two tangent lines is at about 240 nm, which implies that a seriate absorption appears at a higher wavelength than 240 nm in the UV spectrum. Because the PL emission spectra were measured with an excitation wavelength of 230 nm, the deduced absorption region is consistent with the PL optical measurement.

To investigate the band gap structures and corresponding absorption coefficient of the Si NCs, we calculated the band states of Si NCs with both zincblende and ordinary diamond-type structures using first-principles density functional theory with the SIESTA code.[60–62] Electron wave functions were expanded using a double-ζ basis set plus polarization functions.[63] The numerical integrals were performed on a real space grid with an equivalent cutoff of 150 Ry, while the Brillouin zone (BZ) was sampled in a $10\times10\times10$ k-mesh following the Monkhorst-Pack scheme for bulk Si. The structure geometry was based on the obtained crystalline data (Fig. 3, JCPDS Card File No. 800018). The results of the calculations are shown in Fig. 5(c) and 5(d). Fig. 5(c) shows that both the zincblende and diamond-type structures of Si have indirect band gaps, which are indicated by the blue solid line

and red dashed-dotted line, respectively. Interestingly, the calculation reveals band gap broadening, indicated by a red arrow in Fig. 5(c), which could be the origin of violet-blue emission from the Si NCs with a zincblende structure. The absorption coefficient of the Si zincblende structure, which was calculated from the real and imaginary parts of the dielectric constant, is shown in Fig. 5(d), and a schematic diagram of a zincblende crystal framework is shown in its inset. Based on first-principles theory, the main absorption appears around 4.2–5.4 eV, which is less than the result deduced directly from the UV absorption spectrum. Considering that the Si NCs contain numerous stacking fault defects that would influence the absorption behavior, this calculated result confirms that the violet-blue PL emission is induced by the zincblende structure of Si. The optical properties of materials are determined by their energy bands. The surface states, stacking fault defects and size of nanoparticles influence their optical properties by affecting polarization (extrinsic) and the energy band structure (intrinsic). Thus, we conjecture that the PL peaks at 395 and 354 nm (Fig. 5(a)) arise from an unstable exciton transition that is influenced by the distribution of surface states in the sample, which could be caused by the rough or defect-containing surface of the NCs. Accordingly, on the basis of the UV spectra and first-principles calculations, the prominent peak at about 367 nm is assigned as the intrinsic PL peak of Si NCs with a zincblende structure.

C. Annealing of samples and corresponding analysis

To investigate EFLAL using an external electrical field and clarify if the metastable zincblende structure of the resulting Si NCs is the origin of their violet-blue emission, the samples synthesized by EFLAL were annealed in a horizontal high-vacuum stove for 90 min at 600 °C. SEM, XRD, TEM, Raman, and PL measurements were recorded under the same conditions as for the unannealed samples; the results of these measurements are shown in Fig. 6. SEM and TEM analysis (Fig. 6(a) and 6(c), respectively) reveal that the surfaces of the products are glazed, and the size of the particles is in the range of 300–400 nm. These results indicate that annealing removes crystalline defects and increases the size of the Si NCs, producing a stable crystalline structure. The XRD pattern of the annealed sample (Fig. 6(b)) can be completely indexed to a Si phase with diamond-type crystalline structure (JCPDS card 271402). We speculate that the increase in peak intensity compared with that of the unannealed sample is caused by the growth and/or consumption of the small Si NCs during the heating process. The TEM image shown in Fig. 6(c) shows the ripening Si NCs, while the HRTEM image in Fig. 6(d) indicates that the annealed Si NCs possess a diamond structure, because the d value of 0.314 nm is consistent with the typical lattice spacing of (111) crystallographic planes of crystalline Si with a diamond-type structure. Similarly, compared with the Raman spectrum in Fig. 4(b), spectrum in Fig. 6(e) of the annealed Si NCs indicates that crystalline Si with diamond structure has formed. Therefore, annealing converts the metastable zincblende structure in the defect-containing Si NCs to a typical diamond structure. Correspondingly, the PL spectrum of the annealed Si NCs (Fig. 6(f)) does not contain a peak. The structure analysis and PL measurements all suggest that the origin of the violet-blue luminescence is from the Si NCs with a metastable zincblende structure that contains defects.

D. Fabrication mechanism and plausible origin of violet-blue emission

LAL is a rapid process that far from thermodynamic equilibrium.[64] Thus, all stable and metastable phases formed during the initial, intermediate, and final stages of the synthesis process can be preserved in the final products.[42–44,51,65] According to Fabbro and coworkers,[65,66] a large number of Si species with high initial kinetic energy will be generated from the solid target surface and form a dense region during the initial stage of LAL. This is called a laser-induced plasma plume, and it forms in the vicinity of the solid–liquid interface because of the confinement effect of liquid. Then, because the plasma plume is strongly confined in the liquid, the expansion of the plasma plume is delayed to form an adiabatic region.[67] A shock wave is created in this region at supersonic velocity, and this induces extra pressure, called laser-induced pressure. Subsequently, the temperature increases because of the extra pressure in the plasma plume. Therefore, the plasma plume created during LAL at the solid–liquid interface is in a high temperature, high pressure, and

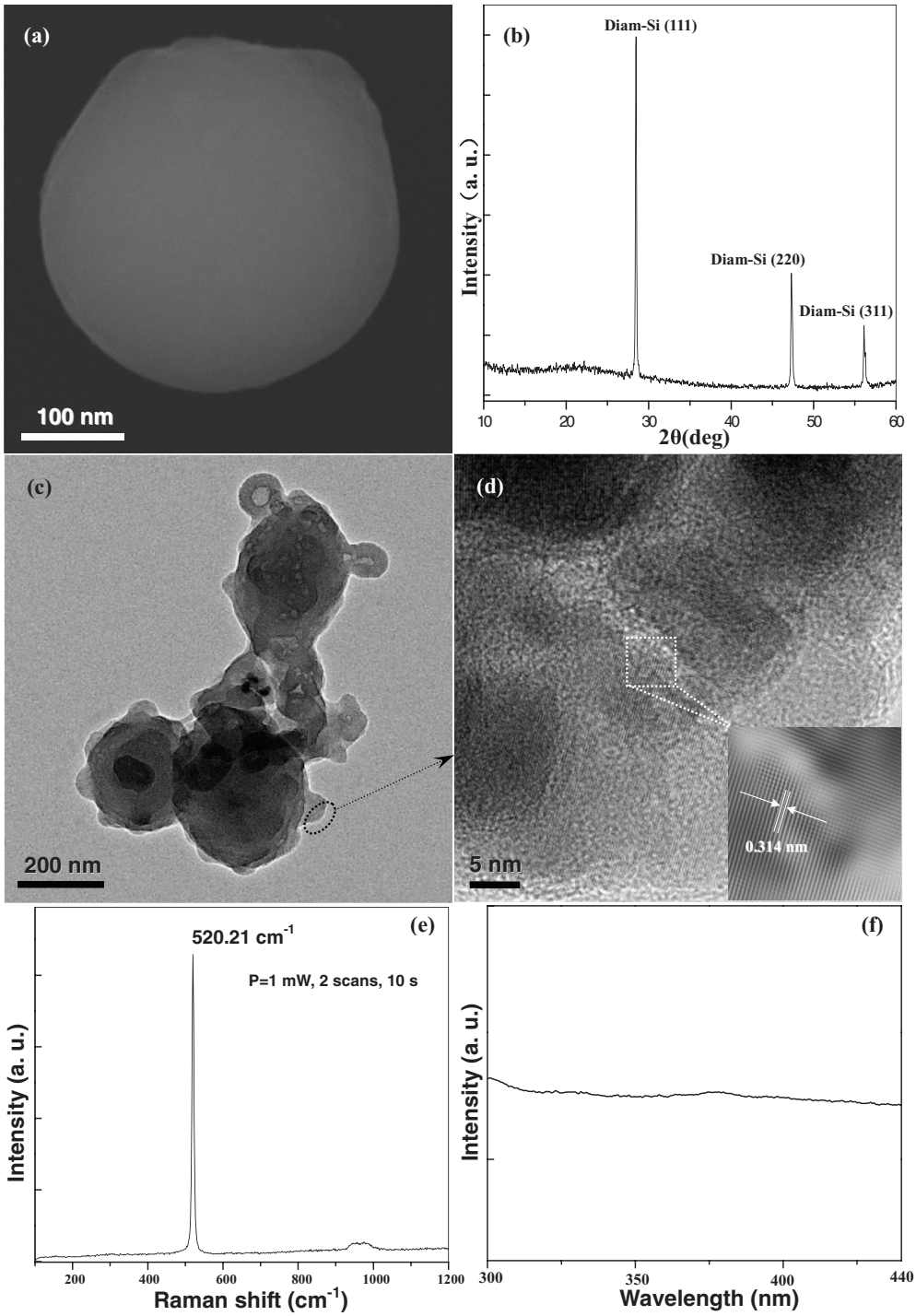

FIG. 6. (a) SEM image, (b) XRD pattern, and (c) TEM image of the annealed sample. (d) HRTEM image of the (111) facet of Si NCs. (e) Raman spectrum of the annealed Si NCs with a laser power density 2 mW. (f) PL spectrum of the annealed Si NCs.

high density (HTHPHD) state, in which the Si species collide with each other to form stable and metastable phases. As a result of the strong confinement effect of liquids, the quenching time of the plasma plume in the liquid is short, so the metastable phase formed during the intermediate stage of the synthesis is found in the final products.

The phase transition of Si from diamond to zincblende structure may take place in the plasma plume within the HTHPHD state. Because LAL is not a thermodynamic equilibrium process, metastable phases can form,[42–44] and thus some Si species from laser ablation may readily transform into Si zincblende structures in the plasma plume within the HTHPHD state by sliding of the crystal basal planes. The particles cool down as the plasma plume condenses in the confining liquid, causing nucleation and growth of the zincblende Si. The small size of the final products is because of the short quenching time. The equilibrium of crystalline phase and structure can be determined by the ambient energy distribution. During LAL, the applied electrical field influences the plasma plume and plays an important role in the growth of defect-containing structures. The applied electrical field could disturb the non-equilibrium process during metastable nucleation, which would influence the final morphology of the products. Importantly, our relevant experimental studies (Fig. 1) show that the applied electrical field affects the formation of defect-containing structures in the products. However, the detailed formation mechanisms of such structures are still unclear; further studies on this topic are underway.

On the basis of the above XRD and HRTEM analysis and the calculated band gaps of the materials, the possibility of the violet-blue luminescence arising from either the SiO_2 component or band-to-band recombination within ordinary Si NCs is safely excluded.[20] The broad emission peak at 366 nm (3.38 eV) is consistent with direct electron–hole recombination at the previously reported Γ point ($\Gamma_{25} \rightarrow \Gamma_{15}$).[68] Moreover, from the UV absorption spectrum (Fig. 5(b)), we can determine that the optical absorption of the synthesized Si NCs for an indirect transition is in a broad UV region, which indicates the existence of the stacking fault effect. According to previous studies, the stacking fault effect not only influences the indirect band gap but also the direct transition energies at Γ or X points.[68] Therefore, the seriate absorption at $<$240 nm implies that the violet-blue emission from the Si NCs is caused by absorption around the UV region, corresponding to direct transitions at the Γ or X points.

Considering the metastable phase of the zincblende structure, the fate of the photoexcited excitons (electron–hole pairs) in Si can be determined by traps and intrinsic recombination processes within the NCs. Generally, the phonon-assisted indirect band gap electron–hole recombination in Si is very weak.[68] However, when a metastable structure is present, the optical band gap is large (Fig. 5(c)), and direct electron-hole recombination at the Γ point ($\Gamma_{25} \rightarrow \Gamma_{15}$) is facilitated, especially because there are numerous stacking fault defects that act as luminescence centers. Subsequent annealing at 600 °C removes a large proportion of crystalline defects in the Si NCs, inducing a crystalline structure, and weakening the blue PL intensity. There may be a small amount of amorphous Si in the product, as confirmed by the XRD result in Fig. 2(d). The effect of these amorphous components on the outer layer of the Si NCs is still not clear and further investigation is needed.

IV. CONCLUSIONS

In summary, metastable Si NCs with zincblende structures were prepared using EFLAL. These Si NCs emit violet-blue light, which disappears upon subsequent annealing of the NCs. However, the violet-blue luminescence of the initial Si NCs remained stable even after aging for 6 months at room temperature. Analysis of the structure and PL measurements of various Si NCs indicated that the violet-blue PL cannot be attributed to a silicon oxide species or quantum confinement effects as in typical Si NCs. We infer that excitons form inside the stacking fault defects in the Si NCs from transitions at the Γ or X points, and then transfer to and recombine at the Γ or X points to emit violet-blue light, which is induced by the metastable phase of Si with a zincblende structure. This mechanism readily explains the disappearance of the violet-blue PL from Si NCs upon thermal annealing. Moreover, understanding the mechanism of violet-blue PL from defect-containing Si NCs with a zincblende structure may be useful in applications such as silicon-based full color displays and biomedical imaging.

ACKNOWLEDGMENTS

The authors thank the National Natural Science Foundation of China (11004253), the China Postdoctoral Science Foundation (201104359), the Natural Science Foundation of Guangdong Province (S2011040001673), the Science Foundation of Guangdong Province under Grant No. sybzzxm201104, and the Ministry of Education (11lgpy60) for supporting this work.

[1] H. Takagi, H. Ogawa, Y. Yamazaki, A. Ishizaki, and T. Nakagiri, Appl. Phys. Lett. **56**, 2379–2380 (1990).
[2] Y. Cui and C. M. Lieber, Science **291**, 851–853 (2001).
[3] F. Erogbogbo, K.-T. Yong, I. Roy, G. Xu, P. N. Prasad, and M. T. Swihart, ACS Nano **2**, 873–878 (2008).
[4] U. Kim, I. Kim, Y. Park, K. Y. Lee, S. Y. Yim, J. G. Park, H. G. Ahn, S. H. Park, and H. J. Choi, ACS Nano **5**, 2176–2181 (2011).
[5] J. C. She, S. Z. Deng, N. S. Xu, R. H. Yao, and J. Chen, Appl. Phys. Lett **88**, 013112 (2006).
[6] L. Fletcher and P. Mitchell, Nature Biotechnology **20**, 351 (2002).
[7] H. Föll, H. Hartz, E. Ossei-Wusu, J. Carstensen, and O. Riemenschneider, Phys. Status Solidi RRL **4**, 4–6 (2010).
[8] L. Pavesi, L. D. Negro, C. Mazzoleni, G. Franzo, and F. Priolo, Nature **408**, 440–444 (2000).
[9] Y. Kanemitsu and K. Suzuki, Phys. Rev. B **51**, 10666–10670 (1995).
[10] J. R. Siekierzycka, M. R. Vasic, H. Zuihof, and A. Brouwer, J. Phys. Chem. C **115**, 20888–20895 (2011).
[11] Z. H. Cen, J. Xu, Y. S. Liu, W. Li, L. Xu, Z. Y. Ma, X. F. Huang, and K. J. Chen, Appl. Phys. Lett. **89**, 163107 (2006).
[12] S. S. Walavalkar, C. E. Hofmann, A. P. Homyk, M. D. Henry, H. A. Atwater, and A. Scherer, Nano Lett. **10**, 4423–4428 (2010).
[13] Takaaki Orii, Makoto Hirasawa, and Takafumi Seto, Appl. Phys. Lett. **83**, 3395–3397 (2003).
[14] V. Švrček, T. Sasaki, Y. Shimizu, and N. Koshizaki, Appl. Phys. Lett. **89**, 213113 (2006).
[15] R. Intartaglia, K. Bagga, F. Brandi, G. Das, A. Genovese, E. Di Fabrizio, and A. Diaspro, J. Phys. Chem. C **115**, 5102–5107 (2011).
[16] T. Yoshida, Y. Yamada, and T. Orii, J. Appl. Phys. **83**, 5427–5432 (1998).
[17] S. W. Lin and D. H. Chen, Small **5**, 72–76 (2009).
[18] J. Y. Fan and P. K. Chu, Small **6**, 2080–2098 (2010).
[19] R. M. Sankaran, D. Holunga, R. C. Flagan, and K. P. Giapis, Nano Lett. **5**, 537–534 (2005).
[20] S. K. Yang, W. Z. Li, B. Q. Cao, H. B. Zeng, and W. P. Cai, J. Phys. Chem. C **115**, 21056–21062 (2011).
[21] S. Furukawa and T. Miyasato, Phys. Rev. B **38**, 5726–5729 (1988).
[22] H. Takagi, H. Ogawa, Y. Yamazaki, A. Ishizaki, and T. Nakagiri, Appl. Phys. Lett. **56**, 2379–2380 (1990).
[23] G. Belomoin, J. Therrien, A. Smith, S. Rao, R. Twesten, S. Chaieb, M. H. Nayfeh, L. Wagner, and L. Mitas, Appl. Phys. Lett. **80**, 841–843 (2002).
[24] Z. Y. Zhou, L. Brus, and R. Friesner, Nano Lett. **3**, 163–167 (2003).
[25] G. G. Qin and Y. J. Li, Phys. Rev. B **68**, 085309 (2003).
[26] E. Rogozhina, G. Belomoin, A. Smith, L. Abuhassan, N. Barry, O. Akcakir, P. V. Braun, and M. H. Nayfeh, Appl. Phys. Lett. **78**, 3711–3713 (2001).
[27] Y. Q. Wang, R. Smirani, and G. G. Ross, Appl. Phys. Lett. **86**, 221920 (2005).
[28] G. W. Yang, J. B. Wang, and Q. X. Liu, J. Phys.: Condens. Matter **10**, 7923 (1998).
[29] J. B. Wang and G. W. Yang, J. Phys.: Condens. Matter **11**, 7089 (1998).
[30] G. W. Yang and J. B. Wang, Appl. Phys A **71**, 343 (2000).
[31] G. W. Yang and J. B. Wang, Appl. Phys. A **72**, 475 (2001).
[32] J. B. Wang, C. Y. Zhang, X. L. Zhong, and G. W. Yang, Chem. Phys. Lett. **361**, 86 (2002).
[33] J. B. Wang, G. W. Yang, and C. Y. Zhang, Chem. Phys. Lett. **373**, 56 (2003).
[34] G. W. Yang, Prog. Mater. Sci. **52**, 648 (2007).
[35] V. Amendola, P. Riello, and M. Meneghetti, J. Phys. Chem. C **115**, 5140–5146 (2011).
[36] X. Y. Li, A. Pyatenko, Y. Shimizu, H. Q. Wang, K. Koga, and N. Koshizaki, Langmuir **27**, 5076–5080 (2011).
[37] F. Lin, J. Yang, S. H. Lu, K. Y. Niu, Y. Liu, J. Sun, and X. W. Du, J. Mater. Chem. **20**, 1103–1106 (2010).
[38] P. Liu, Y. Liang, X. Z. Lin, C. X. Wang, and G. W. Yang, ACS Nano **5**, 4748–4755 (2011).
[39] S. Besner, A. V. Kabashin, F. M. Winnik, and M. Meunier, Appl. Phys. A **93**, 955–959 (2008).
[40] S. K. Yang, W. P. Cai, H. W. Zhang, X. X. Xu, and H. B. Zeng, J. Phys. Chem. C **20**, 19091–19095 (2009).
[41] X. Y. Chen, H. Cui, P. Liu, and G. W. Yang, Chem. Mater. **20**, 2035–2038 (2008).
[42] P. Liu, H. Cui, and G. W. Yang, Cryst. Growth. Des. **8**, 581–586 (2008).
[43] P. Liu, Y. L. Cao, C. X. Wang, X. Y. Chen, and G. W. Yang, Nano Lett. **8**, 2570–2575 (2008).
[44] P Liu, Y. L. Cao, X. Y. Chen, and G. W. Yang, Cryst. Growth. Des. **9**, 1390–1393 (2009).
[45] P. Liu, C. X. Wang, X. Y. Chen, and G. W. Yang, J. Phys. Chem. C **112**, 13450–13456 (2008).
[46] T. E. Itina, J. Phys. Chem. C **115**, 5044–5048 (2011).
[47] K. Hata, S. Yoshida, M. Fujita, S. Yasuda, T. Makimura, K. Murakami, and H. Shigekawa, J. Phys. Chem. B **105**, 10842–10846 (2001).
[48] J. Zou, R. K. Baldwin, K. A. Pettigrew, and S. M. Kauzlarich, Nano Lett. **4**, 1181–1186 (2004).
[49] K. Abderrafi, R. G. Calzada, M. B. Gongalsky, I. Suarez, R. Abarques, V. S. Chirvony, V. Yu. Timoshenko, R. Ibanez, and J. P. Martínez-Pastor, J. Phys. Chem. C **115**, 5147–5151 (2011).
[50] Z. L. Wang, Part. Part. Syst. Charact. **18**, 142 (2001).
[51] P. Liu, Y. L. Cao, H. Cui, X. Y. Chen, and G. W. Yang, Chem. Mater. **20**, 494–502 (2008).

[52] J. Khajehpour, W. A. Daoud, T. Williams, and L. Bourgeois, J. Phys. Chem. C **115**, 22131–22137 (2011).
[53] C. Georgi, M. Hecker, and E. Zschech, J. Appl. Phys. **101**, 123104 (2007).
[54] P. G. Kuzmin, G. A. Shafeev, V. V. Bukin, S. V. Garnov, C. Farcau, R. Carles, B. Warot-Fontrose, V. Guieu, and G. Viau, J. Phys. Chem. C **114**, 15266–15273 (2010).
[55] G. Faraci, S. Gibilisco, A. R. Pennisi, and C. Faraci, J. Appl. Phys. Lett. **109**, 074311 (2011).
[56] H. Ow, D. R. Larson, M. Srivastava, B. A. Baird, W. W. Webb, and U. Wiesner, Nano Lett. **5**, 113–117 (2005).
[57] V. Svrcek, D. Mariotti, T. Nagai, Y. Shibata, I. Turkevych, and M. Kondo, J. Phys. Chem. C **115**, 5084–5093 (2011).
[58] H. Morisaki, F. W. Ping, H. One, and K. Yazawa, J. Appl. Phys. **70**, 1869 (1991).
[59] X. L. Wu,1, S. J. Xiong, G. G. Siu, G. S. Huang, Y. F. Mei, Z. Y. Zhang, S. S. Deng, and C. Tan, Phys. Rev. Lett. **91**, 157402 (2003).
[60] P. Hohenberg and W. Kohn, Phys. Rev. **136**, B864–B871 (1964).
[61] D. Sanchez-Portal, P. Ordejon, E. Artacho, and J. M. Soler, Int. J. Quantum Chem. **65**, 453–461 (1997).
[62] J. M. Soler, E. Artacho, J. D. Gale, A. Garcia, J. Junquera, P. Ordejon, and D. Sanchez-Portal, J. Phys.: Condens. Matter **14**, 2745–2779 (2002).
[63] P. Ordejon and J. M. Soler, Phys. Rev. B **53**, R10441–R10444 (1996).
[64] P. Liu, H. Cui, C. X. Wang, and G. W. Yang, Phys. Chem. Chem. Phys. **12**, 3942–3952 (2010).
[65] A. Sollier, L. Berthe, and R. Fabbro, Eur. Phys. J. Appl. Phys **16**, 131–139 (2001).
[66] L. Berthe, R. Fabbro, P. Peyer, and E. Bartnicki, J. Appl. Phys. **85**, 7552–7555 (1999).
[67] C. X. Wang, P. Liu, H. Cui, and G. W. Yang, Appl. Phys. Lett **87**, 201913 (2005).
[68] J. P. Wilcoxon, G. A. Samara, and P. N. Provencio, Phys. Rev. B **60**, 2704–2714 (1999).